paratus for oxygen evolution and the ferredoxin intermediate pathway for CO_2 reduction. The catalytic process needed for oxygen evolution from water splitting, the possible role of two-photon mechanisms in photosynthesis,[7,47] and the effects of pheophytin and ferredoxin in mediating CO_2 reduction by hydrogen from water splitting are the subject of investigations in succeeding papers of this series.

Acknowledgment. The work reported in this paper was supported by the Basic Research Division of the Gas Research Institute.

Elementary Reconstitution of the Water Splitting Light Reaction in Photosynthesis. 2. Optical Double Resonance Study of (Chl a·$2H_2O$)$_n$ Two-Photon Interactions in Nonpolar Solutions

A. J. Alfano and F. K. Fong*

Contribution from the Department of Chemistry, Purdue University, West Lafayette, Indiana 47907. *Received October 14, 1981*

Abstract: Two-photon interactions of (Chl a·$2H_2O$)$_n$ in deaerated 1:1 n-pentane–methylcyclohexane solutions are investigated by fluorescence quenching measurements obtained by using time-resolved optical methods. The Chl a triplet state is populated by excitation with a modulated laser beam. The decay of the triplet population is monitored by measuring the quenching of Chl a fluorescence excited by a CW laser beam. The reliability of instrumental response in the dual-excitation fluorescence experiments is ensured by electronic simulations by using a red-light emitting diode simultaneously driven by a 52-Hz waveform and a weaker DC input. Flux dependence measurements are analyzed in terms of the steady-state population of the first excited singlet, S_1, under illumination by both lasers and of the flux density of the modulated laser beam. Experimental criteria are given for identifying the biphotonic mechanism responsible for the observed effects. The rationale for establishing singlet–triplet fusion as the mechanism underlying the observed behavior is provided. The possible significance of the two-photon mechanism in the Chl a water splitting reaction relative to the stereospecific interactions in hydrated Chl a aggregation is discussed.

The interest in the study of in vitro chlorophyll a photoreaction[1-9] has centered on the redox reactivity of the chlorophyll in red light, a property that underscores the remarkable ability of Chl a to transform sunlight into stored chemical energy in photosynthesis. Both metal[3-7] and semiconductor[1,2,8,9] materials have been used as electrodes for Chl a films in photoelectrochemical investigations. The experimental observations are describable in terms of Chl a photoredox reactions with the ambient electrolyte and/or the electrode material. Miyasaka et al. reported[8,9] the observation of photoanodic currents by using SnO_2 as electrode. Their results suggest the direct transfer of electrons from the chlorophyll to the conduction band of SnO_2, compatible with earlier work[1,2] and interpretation.[10,11] By contrast the currents generated by metal-based Chl a multilayers in the presence of water are photocathodic,[3-7] leading to H_2 and O_2 evolution from water splitting.[12-14] The enhancement of Pt/Chl a–H_2O photocathodic action on decreasing the electrolyte pH was observed by several workers[5,15] whose interpretations support a cyclic sequence[13] of Chl a photooxidation and subsequent reduction. The underlying photon mechanisms are of interest. The excitation of monomeric hydrated Chl a, leading to delayed fluorescence instead of photooxidation of the chlorophyll, was attributed to a one-photon process.[16] A one-photon mechanism was proposed for electron transfer from Chl a to the semiconductor electrode, whereas the Chl a water splitting reaction was interpreted in terms of a biphotonic process.[13] In this connection the possible involvement of a two-photon mechanism in the primary light reaction in plant photosynthesis was considered.[5,13] One plausible mechanism is singlet–triplet fusion resulting from annihilation,[17] through Förster energy transfer,[18] of the S_1 state of one Chl a molecule by the T_1 state of a second Chl a molecule.[19] In this work we investigate the possible origins for observations by several authors of biphotonic Chl a effects.[13,20,21]

Steady-state analyses[13,14] of Chl a photon mechanisms do not lend themselves to detailed molecular interpretations. Accordingly, we employ the time-resolved fluorescence quenching experiment designed previously in this laboratory for the delineation of Chl a photon mechanisms.[21] In this experiment optical double-resonance techniques are used. The Chl a triplet state is populated by means of a modulated laser beam. The decay of the triplet population is monitored by measuring the quenching of fluores-

(1) H. Tributsch and M. Calvin, *Photochem. Photobiol.*, **14**, 94 (1971).
(2) H. Tributsch, *Photochem. Photobiol.*, **16**, 261 (1972).
(3) F. K. Fong and N. Winograd, *J. Am. Chem. Soc.*, **98**, 2287 (1976).
(4) F. Takahashi and R. Kikuchi, *Biophys. Biochim. Acta*, **430**, 430 (1976).
(5) F. K. Fong, J. S. Polles, L. Galloway, and D. R. Fruge, *J. Am. Chem. Soc.*, **99**, 5802 (1977).
(6) J. G. Villar, *J. Bioenerg. Biomembr.*, **8**, 199 (1976).
(7) L. M. Fetterman, L. Galloway, N. Winograd, and F. K. Fong, *J. Am. Chem. Soc.*, **99**, 653 (1977).
(8) T. Miyasaka, T. Watanabe, A. Fujishima, and K. Honda, *J. Am. Chem. Soc.*, **100**, 6657 (1978).
(9) T. Miyasaka, T. Watanabe, A. Fujishima, and K. Honda, *Nature (London)*, **277**, 638 (1979).
(10) R. Memming, *Photochem. Photobiol.*, **16**, 325 (1972).
(11) H. Kuhn, *Naturwissenschaften*, **54**, 429 (1967).
(12) F. K. Fong and L. Galloway, *J. Am. Chem. Soc.*, **100**, 3594 (1978).
(13) L. Galloway, J. Roettger, D. R. Fruge, and F. K. Fong, *J. Am. Chem. Soc.*, **100**, 4635 (1978).
(14) T. Watanabe and K. Honda, *J. Am. Chem. Soc.*, **102**, 370 (1980).
(15) T. Miyasaka and K. Honda, *Surface Sci.*, in press.
(16) F. K. Fong, L. Galloway, T. G. Matthews, F. E. Lytle, A. J. Hoff, and F. A. Brinkman, *J. Am. Chem. Soc.*, preceding paper in this issue.
(17) F. K. Fong, *Proc. Natl. Acad. Sci. U.S.A.*, **71**, 3692 (1974).
(18) Th. Förster, *Ann. Phys.*, **2**, 551 (1948).
(19) T. S. Rahman and R. S. Knox, *Phys. Status Solidi B*, **58**, 715 (1973).
(20) A. F. Janzen and J. R. Bolton, *J. Am. Chem. Soc.*, **101**, 6342 (1979).
(21) E. R. Menzel, *Chem. Phys. Lett.*, **26**, 45 (1974).

0002-7863/82/1504-2767$01.25/0

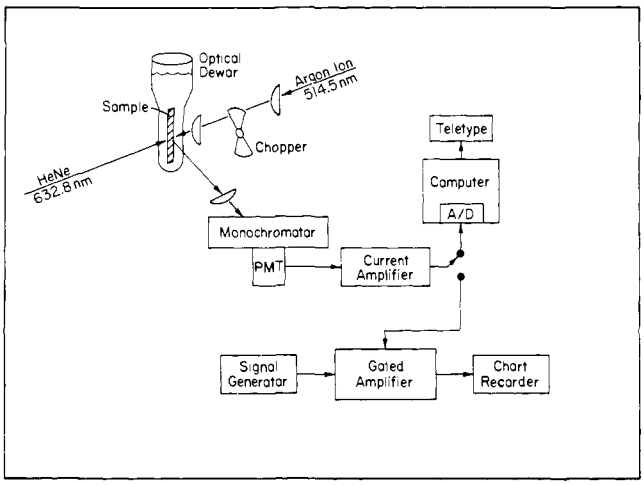

Figure 1. Experimental arrangement used to obtain fluorescence spectra and to perform fluorescence quenching studies. The output of the current amplifier is directed as shown for the latter studies. The current amplifier output is switched to the gated amplifier for the measurement of fluorescence spectra.

cence excited by a CW laser beam. Complications such as the production of Chl *a* radical cations[22] and Chl *a* triplet quenching[23] resulting from the presence of oxygen impurities are minimized by using deaerated Chl *a* samples. Detection-system reliability is ensured by simulation of the instrumental response characteristics using a red-light emitting diode simultaneously driven by a 52-Hz waveform and a weaker DC input. Flux dependence measurements are analyzed in terms of several conceivable photon mechanisms. In conclusion the rationale is provided for establishing singlet–triplet fusion as the mechanism responsible for the observed effects.

Experimental Methods

Stock solutions of chlorophyll *a* in water-saturated *n*-pentane were prepared from fresh spinach according to the usual column chromatographic procedures.[24] The Chl *a* purity was established from Cary 14 spectrophotometric determinations by using the criteria of absorption maximum wavelengths and blue-red peak absorbance ratios.[25]

Solutions containing mostly monomeric Chl *a* were prepared by dilution of an aliquot of freshly prepared stock solution with an equal volume of methylcyclohexane saturated with doubly distilled water. Samples with increased polycrystalline (Chl $a{\cdot}2H_2O)_n$ content were prepared from stock solutions stored for several weeks at 10 °C under argon atmosphere. The preparations were deoxygenated by freeze–pump–thaw cycling at 77 K and sealed in 4-mm o.d. Pyrex glass tubing under vacuum ($<10^{-4}$ torr). All solutions employed in this study were about 10^{-4} M in Chl *a* concentration. The samples were stored at 77 K in the dark.

Fluorescence spectra were obtained after immersing the chlorophyll samples in an optical Dewar filled with liquid nitrogen. Fluorescence was excited by using either a Coherent CR-80-2 He-Ne laser (2-mW CW at 632.8 nm) or an unchopped, unfocused Coherent Model 53 argon ion laser operating CW on the 514.5-nm line at 5.2 mW. The detection equipment is block-diagrammed in Figure 1. Focused fluorescent radiation was passed through a Corning CS 2-58 sharp-cutoff filter onto the entrance slit of a scanning $^3/_4$-m Spex 1402 double monochromator. The exit slit housing of the double monochromator was positioned so that the fluorescence was dispersed by only one grating in order to increase throughput. An RCA 7265 photomultiplier (S-20) cooled to −68 °C served as the detector. The photomultiplier (PMT) was wired according to RCA recommendations for the dynode circuit of a 14-stage tube.[26] The PMT anode current was converted to a voltage by a Keithley 427 current amplifier (0.01-ms rise time) and was directed to a gated amplifier consisting of a Keithley 881 linear gate and 882 scan delay generator. The gate triggering rate was established by a Wavetek Model 130 signal generator. Triggering rate, gate width, and gate time constant conditions were so chosen that the time spent on each nanometer of the fluorescence spectrum by the scanning monochromator was greater than five time constants of the gated amplifier. The output of the gated amplifier was delivered to a strip chart recorder to obtain the traces reproduced in Figure 2.

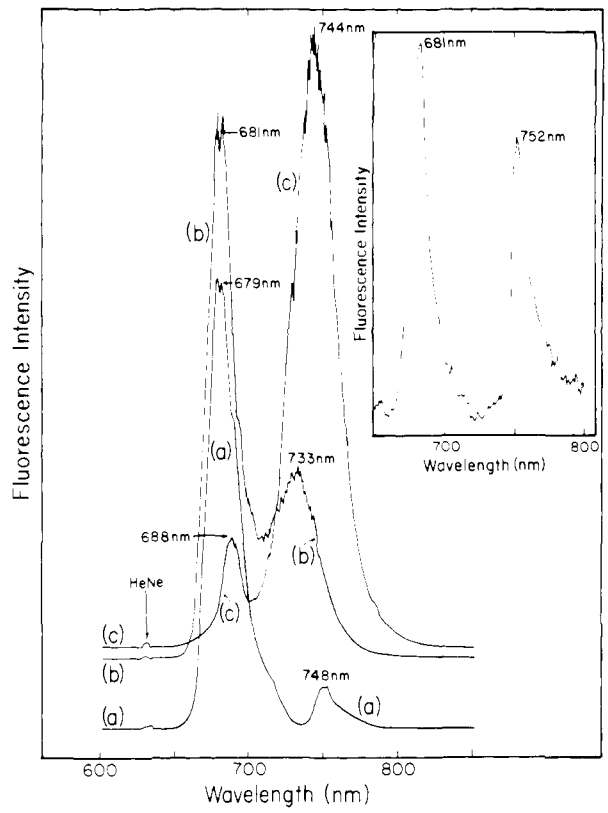

Figure 2. 77-K fluorescence spectra of deoxygenated chlorophyll *a* solutions in 1:1 methylcyclohexane–*n*-pentane. Traces a–c were obtained from samples containing progressively larger amounts of $(\text{Chl } a{\cdot}2H_2O)_n$. Recorder amplification is not constant. Traces a–c were obtained with 632.8-nm He–Ne laser source and the inset was obtained with a 514.5-nm Ar^+ laser source. The inset and trace a were obtained from the same sample. The storage times of the stock solutions used to prepare samples b and c were 6 and 8 weeks, respectively.

Fluorescence quenching measurements were made at fixed monochromator wavelengths corresponding to the sample fluorescence maxima. This was accomplished by simultaneously irradiating the chlorophyll sample (quench cooled to 77 K) with the continuous 632.8-nm and the chopped 514.5-nm outputs of the He–Ne and Ar ion lasers, respectively. The two laser beams were oppositely directed at the sample, and the fluorescence signal at right angles to the excitation sources was focused through a Corning CS 2-58 filter onto the monochromator. Careful alignment of the lasers was necessary to ensure coincident excitation of the sample by both sources. The amplified fluorescence signal was digitized with a 9-bit successive approximation analog to digital (A/D) converter with a 17-μs conversion time (see Figure 1). Input to the A/D converter was limited to ±1 V by a clipping circuit with a <2-μs recovery time after 1000% overload. A Digital Equipment Corporation PDP-8 computer was triggered by the mechanical light chopper to initiate digitization and sampling of the fluorescence signal just prior to the Ar^+ laser cutoff. Sampling was continued up to 11.6 ms after the Ar^+ laser was blocked by the chopper. Typically, 500 repetitions were sampled at 184 μs/point, stored, averaged, and output to a teletype. The chopping rate was 42 Hz.

Experiments designed to test instrument response to the fluorescence signals were carried out with the aid of the simulation circuitry shown in Figure 3. The pulsed emission of a red MV 5022 light-emitting diode (LED) at 680 nm was used as simulated sample fluorescence. Emission from the LED caused by the 52-Hz waveform duplicates the effect of irradiating a chlorophyll sample with the chopped Ar^+ laser. Simultaneously driving the LED with the pulsed signal and the weaker DC input generates an emission to simulate sample fluorescence excited by the CW He–Ne and chopped Ar^+ lasers. The 52-Hz signal was derived from the output of a 21.000 MHz Motorola K1100A crystal oscillator after di-

(22) G. Sherman and E. Fujimori, *Nature (London)*, *219*, 375 (1968).
(23) E. Fujimori and R. Livingston, *Nature (London)*, **180**, 1036 (1957).
(24) (a) H. H. Strain and W. A. Svec in "The Chlorophylls", L. P. Vernon and G. R. Seeley, Eds., Academic Press, New York, 1966, p 21; (b) F. K. Fong and V. J. Koester, *Biochim. Biophys. Acta*, **423**, 52 (1976).
(25) H. H. Strain, M. R. Thomas, and J. J. Katz, *Biochim. Biophys. Acta*, **75**, 306 (1963).
(26) RCA Technical Publication PIT-700B, Dec 1971, Harrison, NJ, pp 8–9.

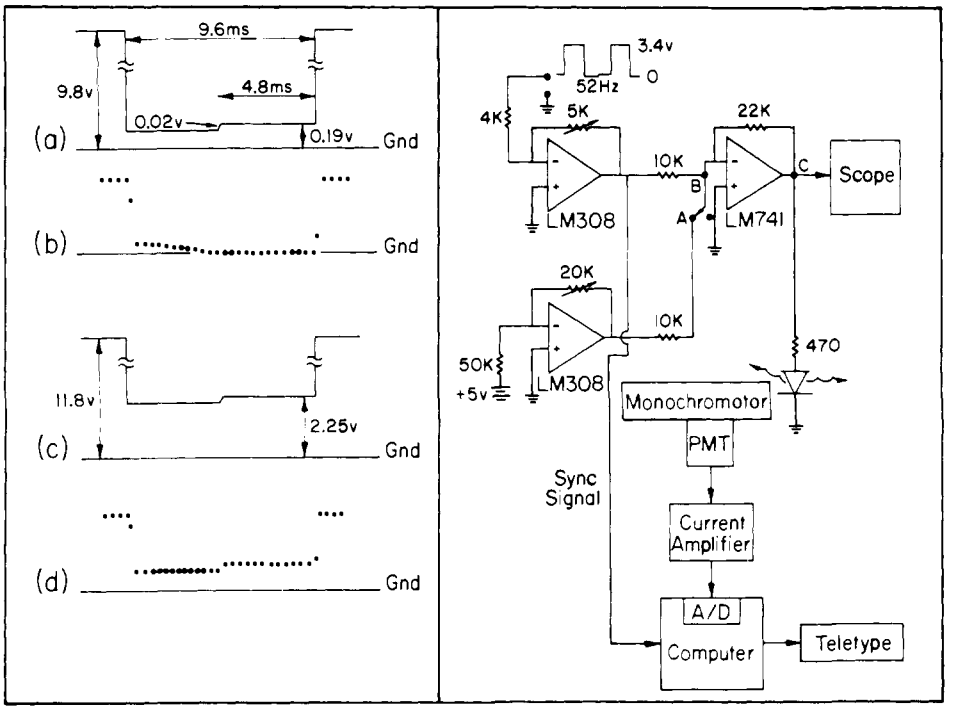

Figure 3. Circuitry to simulate fluorescence signals and detector response of the experimental system in Figure 1: (a) signal at point C in the circuit with only signal B connected; (b) digitized emission of the LED resulting from signal in a, (c) signal at point C in the circuit with signals B and A connected; (d) digitized emission of the LED resulting from signal in c.

vision by five concatenated SN 7490 decade counters and two SN 7476 flip flops.

Experimental Results

(1) Fluorescence Spectra. Fluorescence spectra excited with 632.8-nm He–Ne laser radiation are shown for three quench-cooled 10^{-4} M chlorophyll samples in Figure 2a–c. The growth of the unsymmetrical feature in the 700- to 800-nm wavelength region of these spectra reflects the increased Chl *a* aggregation on aging of the stock solution from which the samples were made. This long-wavelength feature is attributable to polymer (Chl $a{\cdot}2H_2O)_n$ fluorescence.[16] Fluorescence in the 660- to 700-nm wavelength region is due to monomeric Chl *a*. The possibility of observing fluorescence due to pheophytin *a* impurities in the overlap region of 702 nm is eliminated by the fact that such fluorescence would be discernible in only the most grossly adulterated samples, as indicated by fluorescence spectra of samples intentionally spiked with Pheo *a*. The inset in Figure 2 displays the fluorescence spectrum, excited by unfocused 514.5-nm Ar^+ laser radiation at 5.2-mW power, of the sample responsible for the fluorescence spectrum in Figure 2a. The increased amplification (200×) used to obtain the former spectrum reflects the differences in the optical geometries of the two laser configurations and is also indicative of the reduced Chl *a* absorption coefficient at 514.5 nm compared to that at 632.8 nm. The fact that the extinction coefficient of (Chl $a{\cdot}2H_2O)_n$[27] is diminished at 514.5 nm to a lesser extent relative to that of monomeric Chl *a*[28] is manifested by the notable enhancement of the 752-nm fluorescence in the 514.5-nm excited spectrum over the corresponding fluorescence in the 632.8-nm excited spectrum. The Ar^+ laser is capable of producing over 2 W of 514.5 nm; very strong sample fluorescence is excited in both the polymeric and monomeric Chl *a* below the upper limit of 400 mW used in the fluorescence-quenching experiments. Wavelengths of maximum emission obtained from the spectra in Figure 2 were used in the fluorescence quenching experiments detailed below. The maximum wavelengths and band shapes in the fluorescence spectra were subject to variation as the rapidity of sample cooling was altered. Accordingly, all further experiments were performed on samples, quench cooled to 77 K, immediately after the recording of a fluorescence spectrum in order to preclude unnecessary ambiguity in the assignment and/or choice of wavelength maxima.

(2) Quenching of Fluorescence. In the fluorescence quenching experiments the PMT was exposed to fluorescence in both the strong-pumping and the weak-probing facets of a complete chopping cycle. It is thus necessary to demonstrate the ability of the complete detection system to rapidly and faithfully respond to the largely disparate fluorescent light levels incurred. Although the fluorescence signal generated by the Ar^+ laser is strong, measurements indicate that this typically corresponds to a PMT anode current of less than 3 μA. This is well below the 1-mA limit for this photomultiplier, which would seem to eliminate detector saturation as a possible source of error. Such an error was reportedly a factor in previous work.[21]

The simulation circuit in Figure 3 was designed and breadboarded to provide illumination levels of well-known behavior and of the same magnitude as those generated by Chl *a* samples under actual experimental conditions. Figure 3a displays the waveform detected by an oscilloscope at point C in the simulation circuit when the LM 741 operational amplifier is coupled only to signal B. The voltage indicated causes LED emission, generating a PMT current comparable to that produced by a Chl *a* sample during excitation by the chopped Ar^+ laser. Figure 3b shows the results of 500 averaged repetitions of the resultant LED emission using the computer-based detection system. The points are plotted schematically at roughly one-half the actual data acquisition rate of 184 μs/point. The first and last four points are equivalent to full-scale output of the A/D converter as the input voltage was well above the 1-V clipping limit. Since the forward voltage of the LED is ca. 1.7 V, the trace in Figure 3b should fall instantaneously to base line on the negative-going transition of Figure 3a. The actual slow return to base line indicated in Figure 3b would not be caused by an LED with a light fall time (90%–10%) of 50 ns, and accordingly this effect must be attributed to the detection system.

Figure 3c depicts the waveform detected by the oscilloscope at point C when both signals A and B are fed to the LM 741 operational amplifier in the circuit diagram of Figure 3. The high and low voltage levels in Figure 3c are those sufficient to generate PMT currents matching those typically produced by a Chl *a* sample during irradiation by the CW He–Ne laser and simulta-

(27) See Figure 1 of ref 13.
(28) See, for example, L. P. Vernon and G. R. Seeley, "The Chlorophylls", Academic Press, New York, 1966.

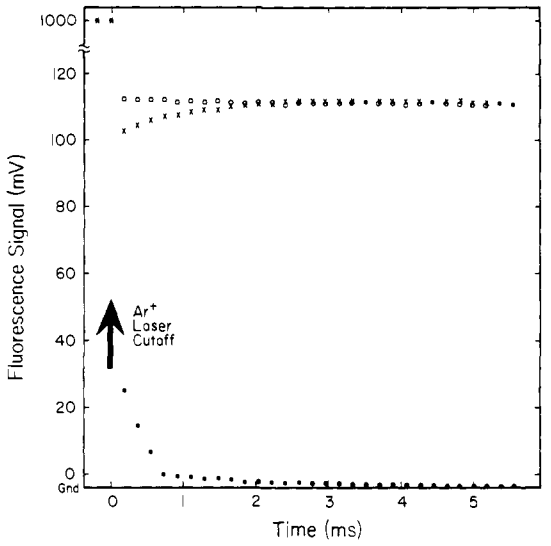

Figure 4. Digitized 733-nm fluorescence of a 10^{-4} M Chl *a* sample under various conditions of illumination: (○) CW He–Ne laser irradiation; (●) chopped Ar^+ laser irradiation; (×) simultaneous irradiation by CW He–Ne and chopped Ar^+ lasers.

neously by the chopped Ar^+ laser. The ensuing LED emission was sampled and averaged for 500 repetitions of the exciting waveform and the result appears as Figure 3d. The points are plotted schematically at approximately one-half the data acquisition rate of 184 μs/point. It is noteworthy that the low-level signal is accurately reproduced as horizontal immediately after the high-light level is terminated. It is also noteworthy that the detection system correctly tracked the very slightly bilevel character of the low level signal. The small voltage differential at the midpoint of the driving waveform responsible for this effect is introduced by a SN 7476 flip flop during the generation of the 52-Hz signal.

These simulations indicate that any slow or sudden change in the fluorescence signal from an actual Chl *a* sample after the Ar^+ laser cutoff in the presence of the CW He–Ne laser can be unambiguously ascribed to sample behavior. It is evident that, in view of Figure 3b, a Chl *a* sample exposed to only the chopped Ar^+ laser should not be interpreted as exhibiting a long-lived fluorescence component if a few milliseconds are required for the base line to be reached after cutoff. Further, on account of the close agreement between the driving waveform (Figure 3c) and the detector output (Figure 3d), there is no need for using the signal generated by only the chopped Ar^+ laser excitation as base-line correction to data obtained with simultaneous irradiation from the two lasers.

Figure 4 demonstrates the results of subjecting the Chl *a* sample, which is responsible for the spectrum in Figure 2b, to various laser illumination conditions with the resulting fluorescence detected at 733 nm. The open circles result from only CW He–Ne excitation and serve as the steady-state fluorescence fiducial level. The points resulting from simultaneous illumination with the CW He–Ne and chopped Ar^+ sources are plotted as crosses. A fluorescence signal less than steady state is indicated at short times after the chopper cutoff. That this effect is attributable to sample fluorescence quenching is clear in view of the simulation given in Figure 3d. Further confirmation is provided by a calculation of the time required for the dynode circuit of the PMT to recover after the Ar^+ laser is cut off by the chopper. This recovery time is estimated at 43 μs on the basis of typical currents supplied by the PMT during the high-light level portion of a chopping cycle. The results from sample illumination with only the chopped Ar^+ laser are shown as solid circles in Figure 4. The observed behavior was forecast by the simulation results shown in Figure 3b. Calculations indicate that the Ar^+ laser is cut off completely within 160 μs by the mechanical chopper so that fluorescence contribution to the slow base-line recovery due to the Ar^+ laser can be safely ruled out.

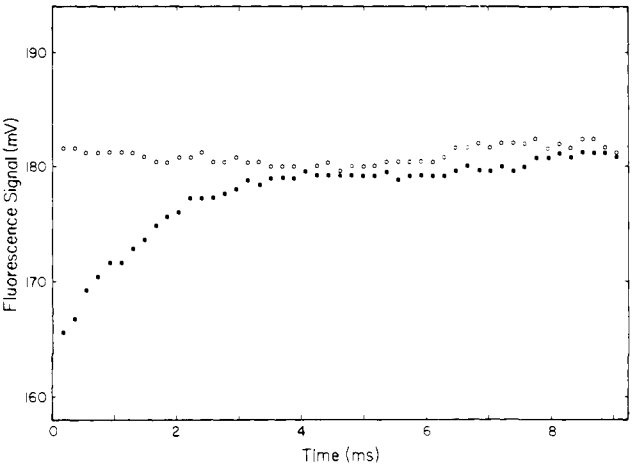

Figure 5. Quenching of 679-nm fluorescence of the sample in Figure 2a: (○) CW He–Ne irradiation; (●) simultaneous irradiation with CW He–Ne and chopped Ar^+ lasers.

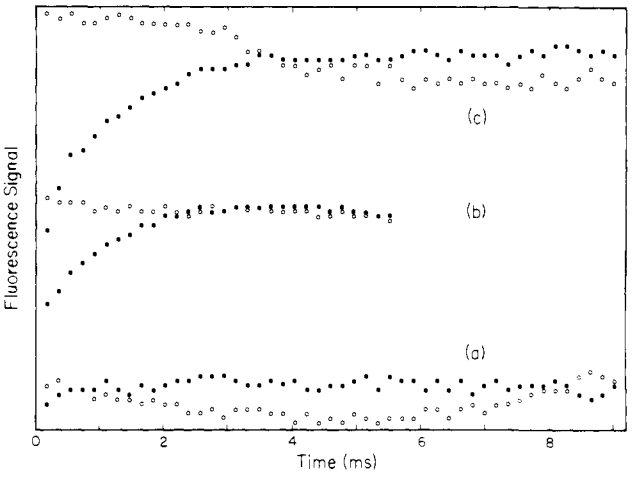

Figure 6. Quenching of polymeric Chl *a* fluorescence of the samples in Figure 2: (a) 748-nm fluorescence corresponding to Figure 2a; (b) 733-nm fluorescence corresponding to Figure 2 b; (c) 744-nm fluorescence corresponding to Figure 2c. The open circles (○) are data points obtained with CW He–Ne laser light. The results of simultaneous irradiation with CW He–Ne and chopped Ar^+ laser are given by ●.

Similar fluorescence quenching results are shown in Figures 5 and 6 for the three samples whose fluorescence spectra appear in Figure 2. Figure 5 shows the quenching effect measured at 679 nm corresponding to the monomeric Chl *a* fluorescence in Figure 2a. Figure 6a depicts the corresponding behavior for polymeric Chl *a* fluorescence at 748 nm. The apparent lack of quenching in Figure 6a may be attributed to the comparatively weak long-wavelength fluorescence component, indicative of the low polymer content of the sample solution. As the content of polymeric Chl *a* in the sample is increased, a corresponding increase in fluorescence quenching is manifested in Figure 6, b and c, for the two samples responsible for Figure 2b,c, respectively.

The sample which exhibited the greatest polymeric Chl *a* content in Figure 2 was used to study the effect of incident Ar^+ laser power on the quenching of fluorescence at 744 nm. The study was conducted at sufficiently low Ar^+ laser power that the data points before the Ar^+ laser cutoff were below the 1000-mV maximum (see Figure 4) of the A/D converter. (In all cases the Ar^+ laser beam was focused, and the corresponding fluorescence exceeded the unfocused He–Ne laser-excited fluorescence by 50–500%.) In the discussion to follow it is shown that these data points reflect steady-state S_1 populations, providing information on the photon mechanisms in addition to that provided by power measurements on the Ar^+ laser beam itself. Figure 7 shows the recordings for seven different incident Ar^+ fluxes in the 0–140-mW range. The results are plotted beginning with the first point after

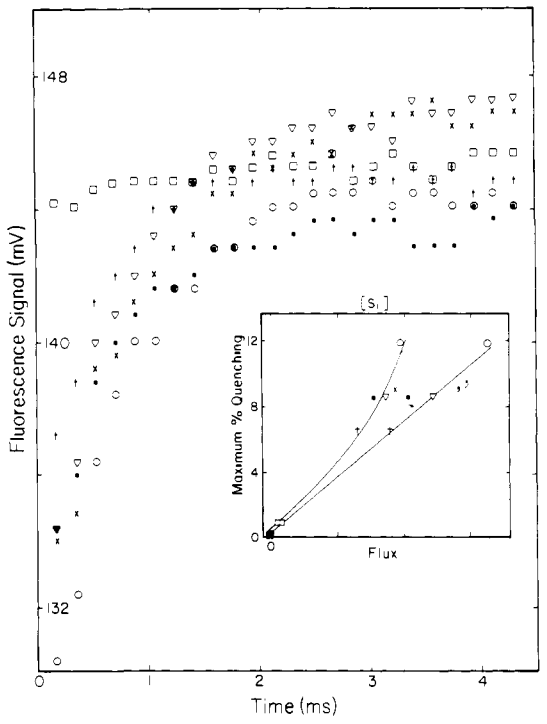

Figure 7. Flux dependence of the fluorescence quenching effect: The range is given by (○) 140 mW and (□) 3.2-mW power focused at the sample. The order of increasing flux is □ < † < ● < ▽ < × < ○. The inset shows the percentage of maximum quenching for each case plotted against the Ar^+ laser power (Flux) and the steady-state fluorescence, $[S_1]$, prior to that Ar^+ laser cutoff. The contribution to this steady-state fluorescence due to He–Ne laser excitation was subtracted out to permit coincidence of the two zero points in the inset.

the chopper cutoff of the Ar^+ laser beam. Measurements were continued for 7 ms beyond the time frame given in the figure. The inset of Figure 7 illustrates the maximum % quenching plotted against the Ar^+ laser flux (linear relationship) and the S_1 steady-state population, $[S_1]$, prior to the Ar^+ laser cutoff (quadratic relationship). Steady-state quantities obtained under simultaneous He–Ne and Ar^+ laser irradiation are given by the subscripts ss′. The incident Ar^+ laser power or flux is symbolized by I_0'. The values of the ordinate in the inset of Figure 7 are provided by the empirical formula

$$Q_{max} = \frac{(F_{ss} - F_0) \times 100}{F_{ss} - D} \quad (1)$$

where Q_{max} is the maximum percentage of fluorescence quenching, F_0 is the first point after the Ar^+ laser cutoff, D is the base-line subtraction for the PMT dark signal, and F_{ss} is the steady-state fluorescence at long times after the Ar^+ cutoff. The same value of F_{ss} was used for all experiments in the flux dependence calculations. This was taken as the average value of the fluorescence signal from 7.9 to 11.6 ms after the Ar^+ laser cutoff for all determinations. The quenching effect as calculated with eq 1 is linear in I_0' with a correlation coefficient of 0.98. The quenching effect is also quadratic in $[S_1]_{ss'}$. This is verified by obtaining a linear fit of Q_{max} with $[S_1]_{ss'}^2$ which yields a correlation coefficient of 0.97.

Discussion

The Chl *a* triplet state has a lifetime on the order of several milliseconds.[29] The millisecond time scale required for restoring the fluorescence to its steady-state value, F_{ss}, after the Ar^+ laser cutoff (see Figure 5–7) thus suggests that a significant population of excited-state Chl *a* is stored in a long-lived triplet state during simultaneous irradiation by the two laser sources. This observation can be readily rationalized by imaging that, immediately after the Ar^+ laser cutoff, the He–Ne laser excites fluorescence in a sample whose effective concentration is diminished by the number of molecules populating the long-lived, nonradiative state. The recovery to a new steady-state fluorescence under He–Ne illumination reflects the reestablishment of equilibrium as the excess triplet population returns to the singlet manifold. This sequence requires the following minimal photophysical mechanism, in the absence of two-photon effects,

$$S_0 + h\nu, h\nu' \xrightarrow{k_a, k_{a'}} S_1 \qquad W_a = k_a I_0 + k_{a'} I_0' \quad (2a)$$

$$S_1 \xrightarrow{k_b} S_0 + h\nu_F \qquad W_b = k_b[S_1] \quad (2b)$$

$$S_1 \xrightarrow{k_{isc}} T_1 \qquad W_c = k_{isc}[S_1] \quad (2c)$$

$$T_1 \xrightarrow{k_d} S_0 \qquad W_d = k_d[T_1] \quad (2d)$$

where $h\nu$ and $h\nu'$ denote the two laser excitations, $h\nu_F$ is the fluorescence quantum, k_a, k_b, k_{isc}, and k_d are the rate constants for the absorption, fluorescence, intersystem crossing, and triplet decay processes, respectively. Equation 1 is recast into the following equivalent form to connect with the fluorescence quenching flux-dependence measurements:

$$Q_{max}/100 = 1 - \left(\frac{\phi[S_1]_0 - D}{\phi[S_1]_{ss} - D}\right) \simeq 1 - \left(\frac{\phi(C - [S_0]_0 - [T_1]_{ss'} - \alpha[S_1]_{ss'}) - D}{\phi[S_1]_{ss} - D}\right) \quad (3)$$

with

$$[S_1]_0 = C - [S_0]_0 - [T_1]_0 \quad (4)$$

and

$$[T_1]_0 \simeq [T_1]_{ss'} + \alpha[S_1]_{ss'} \quad (5)$$

The symbol ϕ denotes the fluorescence quantum yield, C refers to the total Chl *a* concentration, and α is the probability of intersystem crossing, given by $k_{isc}/(k_{isc} + k_b)$ according to eq 2. The approximation in eq 5 is due to the finite time, 0.16 ms, required for the Ar^+ laser cutoff, during which process 2d may deplete the T_1 accumulation to a nonnegligible extent. The only terms in eq 3 with explicit dependence on I_0' are those with ss′ subscripts. Solving the steady-state relationships for eq 2 we write

$$I_0' = \{(k_b + k_{isc})[S_1]_{ss'} - k_a I_0\}/k_{a'} \quad (6)$$

and

$$[T_1]_{ss'} = (k_{isc}/k_d)[S_1]_{ss'} \quad (7)$$

On substitution of eq 6 and 7 in eq 3, we observe that the maximum percentage of fluorescence quenching is linear in I_0' and $[S_1]_{ss'}$, contrary to the results shown in the inset of Figure 7.

If two-photon mechanisms, such as triplet–triplet absorption,[30] are taken into consideration in the minimal scheme (eq 2) additional process of the type

$$T_1 + h\nu, h\nu' \xrightarrow{k_e, k_{e'}} T' \qquad W_e = k_e I_0[T_1] + k_{e'} I_0'[T_1] \quad (2e)$$

and

$$T' \xrightarrow{k_f} T_1 \qquad W_f = k_f[T'] \quad (2f)$$

must be included. In eq 2e and f, k_e and k_f refer to the absorption coefficient for triplet absorption and the rate constant for the T′ decay process, respectively. The decay of the doubly excited triplet, T′, could conceivably involve direct relaxation within the triplet manifold or passage through the S_1 state. Instead of eq 3 we now have

$$Q_{max} \simeq 1 - \frac{\phi(C - [S_0]_0 - [T_1]_{ss'} - [T']_{ss'} - \alpha[S_1]_{ss'}) - D}{\phi[S_1]_{ss} - D} \times 100 \quad (8)$$

(29) C. A. Parker and T. A. Joyce, *Photochem. Photobiol.*, **6**, 395 (1967).

(30) H. Linschitz and K. Sarkanen, *J. Am. Chem. Soc.*, **80**, 4826 (1958).

Solving for the steady-state populations we obtain

$$[T_1]_{ss'} = (k_{isc}/k_d)[S_1]_{ss'} \quad (7a)$$

$$[T']_{ss'} = (k_e I_0 + k_{e'} I_c')k_{isc}[S_1]_{ss'}/(k_f k_d) \quad (9)$$

and

$$[S_1]_{ss'} = (k_{a'} I_0' + k_a I_0)/(k_{isc} + k_b) \quad (10)$$

Upon substituing eq 7a, 9, and 10 in eq 8 we arrive at quadratic dependences of Q_{max} in both I_0' and $[S_1]_{ss'}$, again in disagreement with the results in the inset of Figure 7.

On inclusion of singlet–triplet annihilation[17,19] in the photon mechanism, the sequence

$$S_1 + T_1 \xrightarrow{k_{ST}} T' + S_0 \qquad W_g = k_{ST}[S_1][T_1] \quad (2g)$$

and

$$T' \xrightarrow{k_f} T_1 \qquad W_f = k_f[T'] \quad (2f)$$

is obtained. We assume, for the sake of simplicity, that eq 2e is unimportant relative to eq 2g. Solution of eq 2a–g in the steady-state approximation leads to the populations

$$[T_1]_{ss'} = (k_{isc}/k_d)[S_1]_{ss'} \quad (7b)$$

and

$$[T']_{ss'} = (k_{ST}k_{isc}/k_f k_d)[S_1]_{ss'}^2 \quad (11)$$

In this case the steady-state quantity $[S_1]_{ss'}$ is related to I_0' by the expression

$$(k_{ST}k_{isc}/k_d)[S_1]_{ss'}^2 + (k_b + k_{isc})[S_1]_{ss'} = k_a I_0 + k_{a'} I_0' \quad (12)$$

Given the conditions

$$k_b \lesssim k_{isc} \quad (13)$$

$$k_{ST}[S_1]_{ss'} \gg k_d \quad (14)$$

and

$$k_{a'} I_0' > k_a I_0 \quad (15)$$

Equation 12 simplifies to

$$[S_1]_{ss'} \simeq (k_{a'}k_d/k_{ST}k_{isc})^{1/2}(I_0')^{1/2} \quad (16)$$

We further observe that given

$$k_{isc}/k_d \gg 1 \quad (17)$$

and

$$(k_{ST}/k_f)[S_1]_{ss'} \gg 1 \quad (18)$$

eq 7b and 11 yield the inequalities

$$[T']_{ss'} \gg [T_1]_{ss'} \gg [S_1]_{ss'} \quad (19)$$

Using eq 8, 11, 16, and 19 we now find that Q_{max} is approximately given by a quadratic dependence in $[S_1]_{ss'}$ and varies linearly as the Ar^+ laser flux, I_0', in agreement with the results shown in the inset of Figure 7.

Condition 13 is consistent with common knowledge, supported by the low fluorescence quantum yield of (Chl a·$2H_2O)_n$.[16] Condition 14 appears compatible with the calculations by Rahman and Knox.[19,31] The inequality in eq 15 is predicated upon the experimental fact that the Chl a fluorescence excited by the Ar^+ laser exceeds that by the He–Ne laser (see Experimental Results). The 77-K S_1 lifetime of (Chl a·$2H_2O)_n$ is on the order of 10^{-9} s[16] compared to the $\sim 10^{-3}$-s lifetime of the fluorescence quenching (see Figure 6), which may be attributable to the Chl a T_1 lifetime. Accordingly, we have $k_{isc}/k_d \sim 10^6$, providing verification for condition 17. The inequality in eq 18 means that the back-decay of T′ to T_1 is slow compared to the rate of singlet–triplet fusion, requiring possibly a horizontal displacement of the adiabatic potential energy surface caused by a nuclear rearrangement of the doubly excited T′ state.[32] Such a rearrangement could conceivably result from a charge-transfer interaction between Chl a and the surrounding water-saturated solvent cage. It was previously suggested[13] that the two-photon excitation of (Chl a·$2H_2O)_n$ results in the activation of a tautomeric state given by the charge-transfer (CT) complex (Chl a·$2H_2O)_n^+ \cdots H_2O^-$, i.e.,

$$T' \rightarrow (\text{Chl a}\cdot 2H_2O)_n^+ \cdots H_2O^- \quad (2h)$$

In addition to process 2, e and g, we have also considered other possible biphotonic mechanisms, viz., singlet–singlet fusion

$$S_1 + S_1 \xrightarrow{k_{ss}} S_0 + S_2 \qquad W_2 = k_{ss}[S_1][S_1] \quad (2i)$$

direct two-photon absorption

$$S_1 + h\nu,\ h\nu' \xrightarrow{k_j, k_{j'}} S_2 \qquad W_j = (k_j I_0 + k_{j'} I_0')[S_1] \quad (2j)$$

The corresponding steady-state solutions result in mixed dependences on $[S_1]_{ss'}$ and I_0' closely similar to the functional form of eq 12. Process 2, i and j, may become observable at sufficiently high laser intensities.[33] However, the high rates of intersystem crossing and the low quantum yields of fluorescence found in chlorophyll systems do indicate, according to eq 13, 17, and 19, that insufficient concentrations of S_1 may be present for processes 2i and j to be a factor in the present study. The possible involvement of triplet–triplet fusion is suggested by earlier exciton annihilation studies on anthracene crystals.[34]

$$T_1 + T_1 \xrightarrow{K_T} S_0 + S_1 \quad (2k)$$

However, the steady-state analysis, assuming eq 2k, results in a functional dependence of the maximum % quenching that is indistinguishable in the flux and the S_1 population, contrary to the results shown in the inset of Figure 7. The findings reported here thus favor the singlet–triplet mechanism (eq 2g) as the two-photon process responsible for the observed fluorescence quenching effects reproduced in Figures 5–7. Further confirmation of this conclusion would be provided by fitting the shape of fluorescence–time curves from the quenching experiments with the sequence 2a–g. However, the Nyquist sampling theorem[35] indicates that a data acquisition rate faster than the 184-μs/pt rate utilized would be required for a meaningful analysis. This sampling theorem requires digitization of a waveform at greater than twice the frequency of the highest Fourier component. Preliminary analysis of the fluorescence quenching curves in Figure 6 indicates a decay function of a significantly exponential nature. Unfortunately the Fourier spectrum of an exponential waveform contains frequency components from zero to infinity, so strict adherence to the Nyquist theorem would be impossible in this case. Experiments based on suitably faster data acquisition rates are in progress. The results indicate, as do those shown in Figures 5 and 6, the experimental behavior is not easily fitted by a simple decay function. The approximation in eq 15 is obviously not valid in the low Ar^+ laser flux region where the fluorescence due to the Ar^+ laser is comparable in intensity to that due to the He–Ne laser excitation. Accordingly eq 16 should contain additional terms in the low-flux limit according to eq 12. Experiments are being performed to characterize the flux dependence behavior in this limit. Additional work is also in progress to examine the fluorescence quenching effect in the presence of controlled amounts of added triplet quenchers such as β-carotene and molecular oxygen. Although

(31) Using the values 10^3 s^{-1} and 10^{12} l mol^{-1} s^{-1} [19] for k_d and k_{ST}, respectively, we note that this condition is satisfied by a steady-state concentration $[S_1]_{ss'} > 10^{-8}$ M in a 10^{-4} M solution.

(32) F. K. Fong, "Theory of Molecular Relaxation", Wiley-Interscience, New York, 1975, p 260.

(33) A. J. Campillo, R. C. Hyer, T. G. Monger, W. W. Parson, and S. L. Shapiro, *Proc. Natl. Acad. Sci. U.S.A.*, 74, 1997 (1977).

(34) S. D. Babenko et al., *Phys. Status Solidi B*, 45, 91 (1971).

(35) S. D. Stearns, "Ditial Signal Analysis", Hayden Book Co., Inc.: Rochelle Park, NJ, 1975; Chapter 4.

all measurements described above were performed at 77 K for monomers and polymer aggregates of Chl *a*, fluorescence quenching has been observed in various solvents up to 273 K, well above the corresponding glass transition temperatures. A specially prepared sample which yielded almost entirely (Chl *a*·H_2O)$_2$ aggregates upon cooling to 77 K showed similar quenching behavior. Further investigation of the temperature dependence of fluorescence quenching for various aggregates is in progress.

The experimental findings and conclusions reported above have thus unraveled a primary two-photon mechanism that could conceivably play a part in (Chl a·$2H_2O$)$_n$ photoreaction with water. The secondary events of this reaction are manifested by the ESR detection of the redox reaction cycle of the light-induced (Chl a·$2H_2O$)$_n^{+\cdot}$ radical cation and by the observation of photocathodic behavior of the Pt/Chl *a*·H_2O electrode. The close similarity of the fluorescence quenching effects illustrated in Figures 5 and 6 suggests that the two-photon mechanisms discussed above for aggregated Chl *a* may also be relevant considerations in the case of monomeric hydrated Chl a complexes, although any photocatalytic effects attending this latter case have not been identified. The photoexcitation of monomeric hydrated Chl *a* delayed fluorescence, which does not result in photooxidation of the chlorophyll, is ascribable to a one-quantum process.[16] The above observations suggest the possibility that the available Chl *a* two-photon mechanism is an alternative pathway, effective in Chl *a* photochemistry only when redox requirements compatible with the water splitting reaction are satisified by a specific aggregate configuration, such as (Chl *a*·$2H_2O$)$_{n\geq 2}$. In this sense the stereospecific interactions of Chl a–H_2O interactions seem to take on an added significance in the study of the Chl *a* water splitting reaction. In view of eq 19 it is evident that, under steady-state illumination, the chlorophyll is distributed predominantly between the ground-state singlet and the CT complex and that the steady-state populations of S_1 and T_1 are negligibly low. These observations are apparently in agreement with the fact that (Chl *a*·$2H_2O$)$_n$ in homogeneous solutions is only very weakly fluorescent[16] and that in a condensed state, in which k_{ST} is expected to be significantly enhanced,[19] the chlorophyll is nonfluorescent. In this connection it is noteworthy that the fluorescent and the triplet states of the water splitting reaction center Chl *a* in vivo have hitherto not been observed.

Acknowledgment. The work reported in this paper was supported by the Basic Research Division of the Gas Research Institute.

Elementary Reconstitution of the Water Splitting Light Reaction in Photosynthesis. 3. Photooxidative Properties of Chlorophyll Dihydrate on Metal as Catalyst for Water Photolysis

Michael S. Showell and Francis K. Fong*

Contribution from the Department of Chemistry, Purdue University, West Lafayette, Indiana 47907. *Received October 14, 1981*

Abstract: In this work we investigate the photooxidative properties of chlorophyll *a* dihydrate as photocatalyst for the water splitting reaction, using Pt and other metals as nonbiological catalysts for reaction product formation. The photoelectrodeposition of (Chl *a*·$2H_2O$)$_n$ microcrystals from *n*-pentane suspensions on Pt electrodes is described. The formation of a contiguous multilayer of (Chl *a*·$2H_2O$)$_n$ on Pt is examined by means of electron microscopy. The effect of an applied voltage on the electrodeposition process is delineated in terms of the amount of Chl *a* plated and the photocathodic activity of the resulting Pt|Chl *a* electrode. A quantum efficiency of 0.88% was obtained at the red maximum, 735 nm, of the photogalvanic action spectrum. The catalytic function of the metal surface is examined by determining the activity of a Pt|Chl *a*–H_2O photocathode against a series of different counterelectrodes (anodes), viz., Pt, Cu, Fe, and Ni. The order Cu > Ni > Fe > platinized Pt > shiny Pt is established for the relative effectiveness of these metals as counterelectrodes at photocurrent densities $\gtrsim 10^{-1}$ $\mu A/cm^2$ in oxygen-depleted aqueous solutions. The observation of light-induced decay and dark restoration of the photogalvanic activity is numerically fitted to a kinetic model for gaseous product evolution and removal at the electrodes. The apparent reduction potential for a 1:3 mixture of (Chl *a*·$2H_2O$)$_2^{+\cdot}$ and (Chl a·$2H_2O$)$_6^{+\cdot}$ responsible for the observed oxygen evolution from water splitting is determined by potentiostatic and electron spin resonance measurements to be 1.05 V. This observation is attributable to the reduction potential of (Chl *a*·$2H_2O$)$_n^{+\cdot}$.

Photosynthesis in green plants involves two different chlorophyll–protein complexes known as the "P700" and the "P680" reaction centers. The latter is commonly recognized to be directly responsible for the evolution of molecular oxygen from the water splitting reaction in vivo. In recent years there has been an increasing number of investigations in light conversion and photon energy storage using the chlorophyll as photocatalyst in the absence of biological enzymes.[1-14] Observations on the in vitro photosynthetic activity of Chl *a* show that the dimers of chlorophyll *a* monohydrate and dihydrate, (Chl a·H_2O)$_2$ and (Chl *a*·$2H_2O$)$_2$,

(1) T. Miyasaka and K. Honda, in "Photoeffects at Semiconductor-Electrolyte Interface", A. J. Nozik, Ed., American Chemical Society, Washington, DC, 1981, Adv. Chem. Ser. No. 146, p 231.
(2) F. K. Fong, in "Light Reaction Path of Photosynthesis", F. K. Fong, Ed., Springer-Verlag, Heidelberg, West Germany, Chapter 8, in press.
(3) C. W. Tang, F. Douglas, and A. C. Albrecht, *J. Phys. Chem.*, **79**, 2723 (1975).
(4) C. W. Tang and A. C. Albrecht, *J. Chem. Phys.*, **63**, 953 (1975).
(5) J. G. Villar, *J. Bioenerg. Biomembr.*, **8**, 199 (1976).
(6) J. M. Mountz and H. T. Tien, *Photochem. Photobiol.*, **288**, 395 (1978).
(7) H. Ochiai, H. Shibata, A. Fujishima, and K. Honda, *Agric. Biol. Chem.*, **43**, 881 (1979).
(8) T. Miyasaka, T. Watanabe, A. Fujishima, and K. Honda, *Nature (London)*, **277**, 638 (1979).
(9) F. K. Fong and N. Winograd, *J. Am. Chem. Soc.*, **98**, 2287 (1976).
(10) F. Takahashi and R. Kikinchi, *Biochim. Biophys. Acta*, **430**, 490 (1976).
(11) Y. Toyoshima, M. Morino, H. Motoki, and M. Sukigara, *Nature (London)*, **265**, 187 (1977).
(12) T. Miyaska, T. Watanabe, A. Fujishima, and K. Honda, *J. Am. Chem. Soc.*, **100**, 6657 (1978).

0002-7863/82/1504-2773$01.25/0